UNDERGROUND MINING ENGINEERING 46 (2025) 1-15 UDK 62
UNIVERSITY OF BELGRADE - FACULTY OF MINING AND GEOLOGY EISSN 2560-3337

Original scientific paper

INTERPRETATION OF TRANSIENT CAVING DUST PATTERNS DURING SEQUENTIAL CAVING OPERATION IN LTCC FACE

Krishna Tanguturi[1], Rao Balusu[1], Johnny Qin[1], Bharath Belle[234]

Received: May 30, 2024 **Accepted:** June 10, 2025

Abstract: Longwall top coal caving (LTCC) is a mining technology introduced for enhancing the coal production rate by using the top coal caving (TCC) operations for thick seams. LTCC mine increases coal production rates but at the expense of high dust exposure and may create hazardous conditions for mine operators. It is vital for the introduction of advanced dust control technologies as well as strategies during LTCC operations for dust reduction. For developing LTCC dust control strategies, fundamental understanding of transient caving dust flow pattern across the face is necessary. Note, region above the rear armored face conveyor (AFC) is difficult to access for carrying out field measurements and hence numerical approach is the only option left for determining the dust and flow fields. In this paper, an attempt is made to predict respirable dust flow patterns during sequential caving operations in the mid face region using computational fluid dynamics (CFD) techniques. Results predicted caving dust sources entering the downstream chock and dispersing into the walkway region within 5 seconds. Respirable dust in the first downstream walkway remains below 2mg/m³ whereas in the second downstream chock in the sequence is above 2.5mg/m³. Interpreting the results, it can be inferred that caving dust controls using water sprays need to be activated in not only in the caving chock but also in the immediate downstream chock from the start of the sequence caving for preventing the migration respirable dust into the walkway regions of the downstream chocks until the completion of the sequential caving operation in all the five chocks.

Keywords: Respirable dust; top coal caving; sequential caving

[1] CSIRO Mineral Resources BU, Mine Safety and Environment Group, QCAT, QLD, Australia, 4069
[2] School of Mechanical and Mining Engineering, UQ, Australia, 4072; Adjunct Associate Professor
[3] University of Pretoria, Hatfield, Pretoria 0002, South Africa
[4] SIMTARS Australia

E-mails: krishna.tanguturi@csiro.au, ORCID: 0000-0003-4789-3259; rao.balusu@csiro.au, ORCID: 0000-0001-5495-8220; johnny.qin@csiro.au, ORCID: 0000-0001-5495-8220
bharath.belle@simtars.com.au, ORCID: 0000-0002-2467-948X

1 INTRODUCTION

LTCC method is based on the "Soutirage" longwall caving method originally developed in the French underground coal industry. The essential features of the soutirage method are that a conventional height longwall face operates at the base of a thick coal seam. The top coal is mined by allowing it to cave above and immediately behind the rear chock canopy. LTCC chocks are specially designed with various types of hatches or draw point in each, through which the caved coal can pass. Different soutirage methods either passed the caved coal directly onto a second conveyor located within the rear of the chocks, or via a chute between the legs, through to the front AFC (Quang, 2010). LTCC method offers a viable means of extracting up to 75% to 80% of seams in the 5m to 9m thickness range. This method has improved control over spontaneous combustion in thick seams, through removal of most of the top coal from the face (Cai, 2004).

In 2001, CSIRO and University of New South Whales carried out a pre-feasibility study of introduction of LTCC technology for Australian underground coal mines. As part of the study, a risk assessment is carried out on the application of LTCC in Australian condition. In fact, LTCC is viewed to have many advantages compared to high reach single pass longwalls. Some of the points that came out of the risk assessment are poor ventilation for rear AFC resulting in an accumulation of dust and gases, the rear AFC drives exposed to gas made from caving coal with limited ventilation and large dust exposure in the face due to additional caving dust source. CSIRO at QCAT carried out extensive studies on gas modelling in LTCC face and investigated the effects gas distribution in LTCC mines. Various gas control options are investigated using numerical techniques that would successfully eliminate or minimize the methane gas concentrations at the rear AFC regions (Greg, 2007). The modifications and improvements to the LTCC equipment are being carried out and will no doubt result in an industry-leading extraction system capable of maximizing the value of the operation (Greg, 2007). Understanding dust and airflow patterns is crucial for developing effective dust control measures, particularly for managing dust generated by caving at the LTCC face. In recent years, many numerical studies were carried out on dust monitoring and dust dispersion in longwall panels (Ren, 2023), and in gate road development (CRC Press, 2023). Studies focusing exclusively on dust dispersion in LTCC faces are scarce and have yet to be thoroughly investigated, both in the field and through numerical simulations.

Dusts are small solid particles, conventionally taken as those particles below 75μm in diameter, which settle out under their own weight and may remain suspended for some time. Dust particles are frequently found with dimensions considerably below 1 μm and, their settlement due to gravity is negligible. The terminal velocity of a 1 μm particle is about 0.03mm/sec, so movement of the air is more important than sedimentation through it (WHO, 1999). The experimental studies in mines and laboratories indicate that only a very small portion of the dust that is generated gets airborne, which are approximately

0.001 to 0.08 percentages in the respirable dust size range, and 0.01 to 0.12 percentages for the inhalable dust size range (WHO, 1999). The primary dust sources in LTCC face are air intake, stage loader/crusher, front AFC and rear AFC transfer points, shearer, chocks advancement and caving. Of these, three major dust sources are shearer, chocks advancement and caving operations. With the introduction of top coal caving in the longwall face, the numbers of dust sources shoot up to seven. These primary dust source locations along a LTCC face have been accounted for dust generation, as shown in Figure 1.

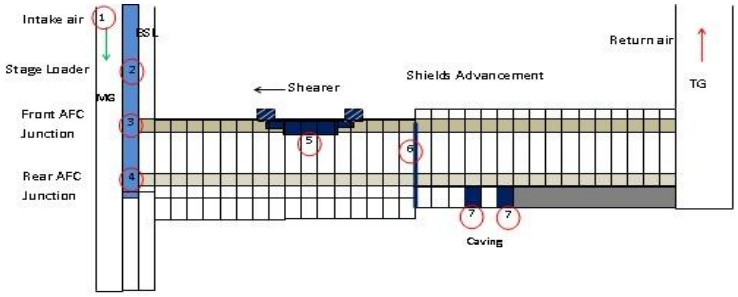

Figure 1 LTCC dust sources at various locations across the face

2 GEOMETRY - MODEL DEVELOPMENT

ANSYS design modeler is used for developing the replication of the LTCC mine. Figure 2 presents an isometric view of the CFD model showing the MG side equipment i.e., beam stage loader (BSL), MG transitional chocks and the main chocks in the LTCC face. In this model, the LTCC face width is 320m, cutting height is 3.6m and the roadway width is 5.6m. For accumulating the respirable dust dispersion into the LTCC goaf, a goaf length of 100m was used in the CFD model.

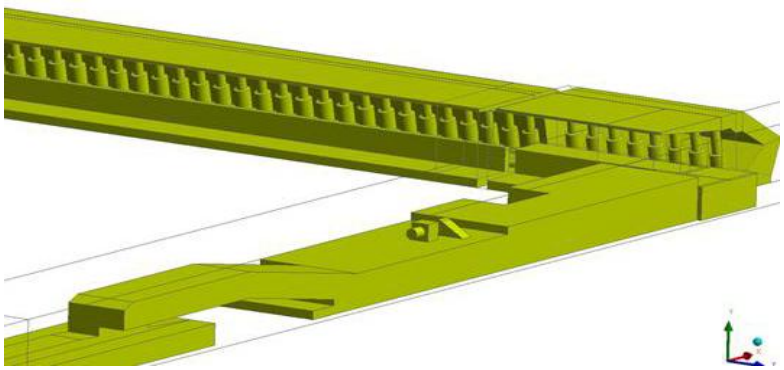

Figure 2 CFD model of the LTCC face

On the MG side of the longwall panel, key components include the BSL, front and rear AFC transfer points, and their corresponding driver units integrated into the first two sets of MG transition chocks. The main chocks (#145) span most of the LTCC face, succeeded by three TG side transitional chocks. The initial two chocks (1-2) primarily reside in the goaf region, housing the rear AFC junction and drive unit. Subsequently, chocks 3-5 of the second MG transition set accommodate the front AFC and its drive unit. The sequence continues with normal chocks 6-149, extending through majority of face region, as illustrated in the cross-sectional view in Figure 3.

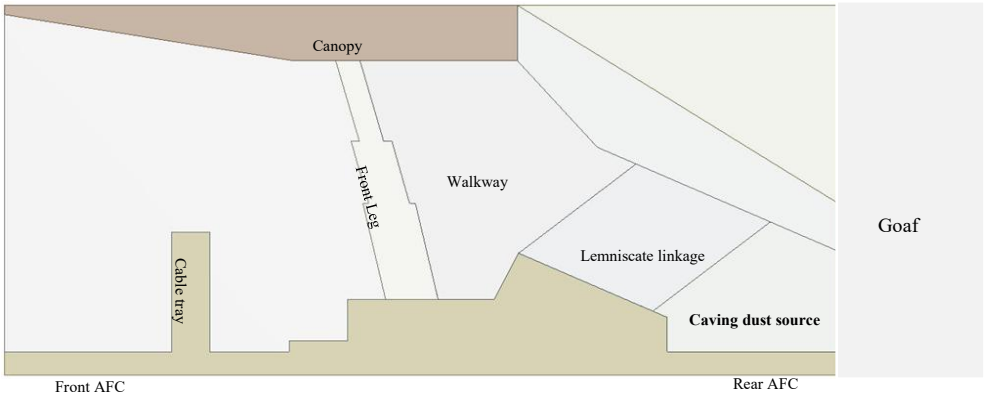

Figure 3 Schematic representation of cross section of the face with the caving dust source

3 CFD - MODEL SETUP

At the MG inlet, velocity inlet boundary condition is specified which corresponds to volume flow rate of 60 m^3/s, while a zero-pressure boundary condition is applied at the tailgate return. Turbulent airflow modelling across the LTCC face is carried out using k-epsilon model. The primary focus of the simulation is to emulate the dispersion patterns of dust particles originating from the caving process. In Ansys Fluent, Discrete Element Model (DEM) (ANSYS, 2023) is activated and respirable particle size distribution ranging between 0.1 to 10µm, with a mean particle size diameter of 5µm is specified. Various forces acting on the particle, i.e., drag force, lift force, and virtual mass force are incorporated in the discrete model. In this numerical model, specifying dust sources is a challenging task, several numerical trials are carried out before the caving dust source is fixed. An approximate dust emission during top coal caving operation is assumed amounting to be 500 mg/s, with a specific allocation of 150 mg/s attributed to respirable dust, a quantity maintained at the caving source continuously for a duration of 10 seconds. At this stage of the project, it is very difficult to quantify the exact caving dust source. It is to be noted here that the caving dust quantity used in the model is just an

assumption and assumes that caving dust could be one third of the shearer dust sources generated during shearer cutting operations.

4 CAVING SEQUENCE

A dynamic modeling approach is employed to simulate the transient flow of dust particles during the top coal caving process in the LTCC face. The specific caving sequence adopted in the LTCC mine is visually represented in Figure 4. The caving operation unfolds successively at five chocks, with each chock facilitating caving for a duration of 10 seconds. The initiation of caving at each chock occurs 5 seconds after the onset of the sequence. Notably, a 5-second overlap is observed, during which caving concurrently takes place at two consecutive chocks. The overall sequence of caving operations across all five chocks extends for a total duration of 30 seconds.

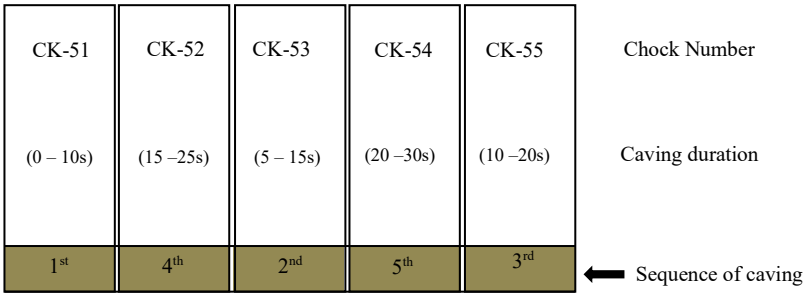

Figure 4 LTCC sequence from chock CK#51 to chock CK#55

5 MODEL VALIDATION

Air velocities and dust profile surveys are carried out using real time airflow and dust readings during normal production conditions at various locations along the face line using thermo scientific personal dust monitor 3700 (PDM 3700), vane anemometer, kestrel 1000 intrinsically air velocity safe meters and gravimetric personal dust samplers. The dust and ventilation data are used as inputs to validate the modelling results.

Figure 5 shows the snapshot of the field measurements containing air velocities, respirable dust and the location of the shearer at the time of measurement.

Location	Sample Point	Date & Time	Air Velocity @Sample Points (m/s)	PDM #1996 @Sample Points (mg/m³)	PDM #0877 @MG Chock 1-2 (mg/m³)	Shearer Position (Chock No.)	Comments
5m up stream of MG Corner (Shearer at mid-face area)	1	23/07/2019 13:10	3.50	0.87	0.98	40	Points 1 to 3 were taken on the top of BSL structure; Point 4 was taken at mid height of the side passage way (about 1-1.2m wide)
	2	23/07/2019 13:12	3.84	0.76	0.94	66	
	3	23/07/2019 13:14	4.24	0.65	0.88	85	
	4	23/07/2019 13:16	3.60	0.57	0.80	93	
10m inbye of MG (Chock #7) 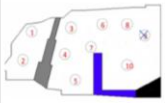	8	23/07/2019 13:19	2.72	0.44	0.64	105	PDM 591 (#0877) fixed at MG Chock #2; Point #9 can't be reached; LW face lost power @13:28; Power back on 13:40
	10	23/07/2019 13:21	4.08	0.32	0.59	117	
	6	23/07/2019 13:23	2.32	0.38	0.48	123	
	7	23/07/2019 13:25	3.35	0.43	0.38	129	
	3	23/07/2019 13:27	4.21	0.48	0.33	134	
	4	23/07/2019 13:28	3.30	0.48	0.32	137	
	5	23/07/2019 13:43	3.14	0.61	0.43	137	
	1	23/07/2019 13:44	1.65	0.49	0.45	137	
	2	23/07/2019 13:45	1.79	0.33	0.46	137	
30m inbye of MG (Chock #17) 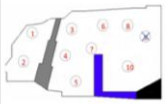	8	23/07/2019 13:48	4.80	0.67	0.52	143	Chock #12 Spray on AFC; Chock #14 Spray from Chock Top to AFC; there are a number of this type of set up along the LW face.
	10	23/07/2019 13:50	4.00	0.78	0.47	144	
	6	23/07/2019 13:52	0.84	0.94	0.43	140	
	7	23/07/2019 13:54	3.70	0.90	0.41	128	
	3	23/07/2019 13:56	3.05	0.77	0.46	127	
	4	23/07/2019 13:58	3.36	0.63	0.48	127	
	5	23/07/2019 13:59	3.48	0.54	0.49	127	
	1	23/07/2019 14:00	1.16	0.47	0.49	127	
	2	23/07/2019 14:02	2.33	0.40	0.49	127	

Figure 5 A Snapshot of field measurements

Figure 6 shows a comparison of field measurements and simulated results at 17th chock, i.e., at approximately 30m from the MG corner. Simulated respirable dust are around 0.4 – 0.9 mg/m³ at this location, which are in close agreement with the field measurements. In walkway, the respirable dust is around 0.7 – 0.9 mg/m³. Both CFD simulation results and the field measured data are in close agreement in various regions of the longwall face at this location.

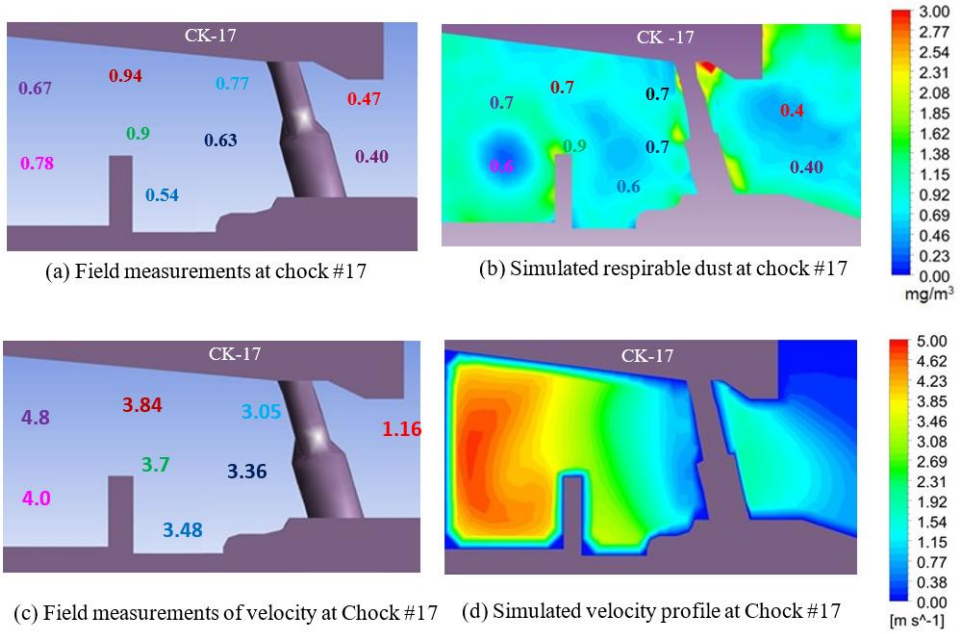

(a) Field measurements at chock #17 (b) Simulated respirable dust at chock #17

(c) Field measurements of velocity at Chock #17 (d) Simulated velocity profile at Chock #17

Figure 6 Field measurements and simulated dust distributions at chock #17

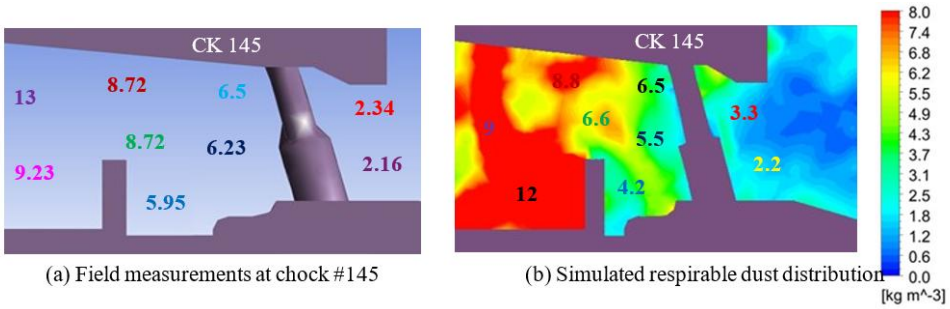

(a) Field measurements at chock #145 (b) Simulated respirable dust distribution

Figure 7 Field measurements and simulated dust distributions at chock #145

Figure 7 illustrates a comparison between field measurements and simulation results in chock145 located at a position 20m from the TG corner. In Figure 7 (a), field measurements reveal elevated respirable dust ranging from 6.0 to 13.0 mg/m³. In the walkway region, respirable dust concentrations hover around 6.0 – 9.0 mg/m³. Concurrently, the modeling indicates that respirable dust in these areas ranges from 4.0 mg/m³ to 12.0 mg/m³. Here, it is crucial to emphasize that the field measurements used for validation originate from the longwall face not from LTTC. The validation process involved conducting simulations that encompass all longwall dust sources within the numerical models.

6 RESULTS AND DISCUSSION

0-10s

Figure 8(a) illustrates the aerial view of the dust particle flow pattern five seconds after the initiation of the first caving sequence at chock 51, with the second caving sequence commencing at chock 53. The results show that the particles spread across the rear AFC of three consecutive chocks and the walkway of four successive downstream chocks. Notably, the movement of dust particles in the low-velocity rear AFC region is slower compared to their motion in the high-velocity walkway region.

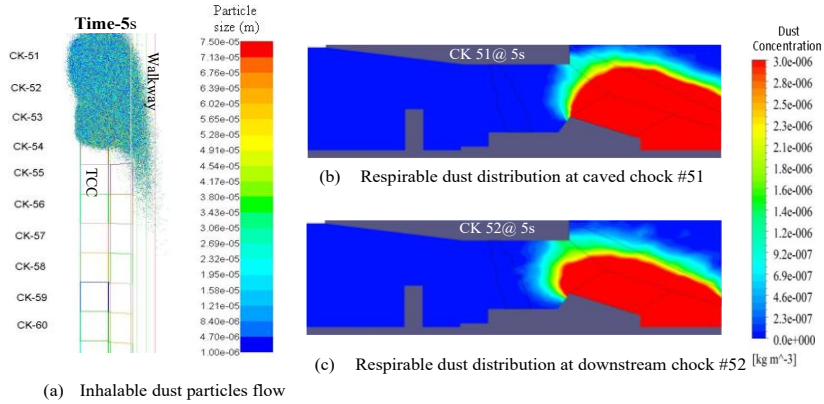

(a) Inhalable dust particles flow

(b) Respirable dust distribution at caved chock #51

(c) Respirable dust distribution at downstream chock #52

Figure 8 Caving dust flow pattern and dust distribution at 5s

Figure 7(b) illustrates the respirable dust at caved chock 51, five seconds into the caving operation. At this location, the walkway is partially covered by dust particles, showing respirable dust of approximately 1.5 mg/m3. A respirable dust cloud originating from the rear AFC region reaches a height of about 2 meters and continues to disperse in all directions.

Figure 8(c) reveals respirable dust at the downstream chock 52. The walkway is predominantly filled with both respirable and inhalable dust particles, and specific regions of the walkway exhibit respirable concentrations surpassing 1.5 mg/m^3. Above the rear AFC region of downstream chock 52, dust completely occupies the space, indicating elevated respirable concentrations exceeding 3 mg/m^3. This underscores the importance of activating dust controls within 5 seconds of initiating the caving sequence in the downstream chock to prevent the migration of dust particles in the walkway region.

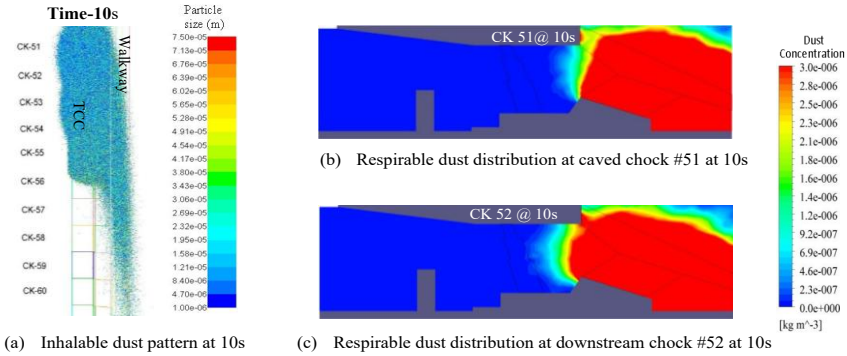

(a) Inhalable dust pattern at 10s

(b) Respirable dust distribution at caved chock #51 at 10s

(c) Respirable dust distribution at downstream chock #52 at 10s

Figure 9 Caving dust flow pattern and dust distribution at 10s

After 10 seconds, marking the conclusion of the caving operation in chock 51, the first chock in the sequential caving sequence, dust particles now envelop the rear AFC in downstream chocks 52-56 and the walkway of downstream supports 52-59, as illustrated in Figure 9 (a). In the caved chock 51, only a segment of the walkway is covered by dust particles, and the respirable dust are below 1.5 mg/m^3, as depicted in Figure 9 (b). From these results, it can be inferred that dust particles enter the caving chock only partially, considering it is the initial chock in the sequential caving operation.

From Figure 9, it can be inferred that dust particles infiltrate the walkway of the immediate downstream chock 52 and the subsequent downstream chocks 53, 54, and 55, exhibiting high respirable dust surpassing 2 mg/m^3 in the walkway. Figure 9 illustrates the dust distributions in downstream chock 55, indicating respirable dust above 2 mg/m^3 in the walkway region. This suggests that respirable dust particles completely migrate into the walkway, while larger particles settle in the rear AFC region of the downstream chocks preceding it.

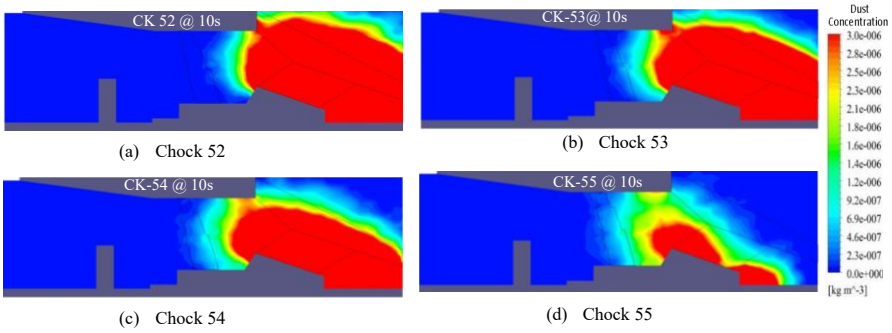

(a) Chock 52 (b) Chock 53

(c) Chock 54 (d) Chock 55

Figure 10 Caving dust distribution at downstream chocks at 10s

11-20s

The third chock in the caving sequence commences at chock #55 and lasts for 10 seconds. At the 15-second mark, the fourth caving chock initiates at chock #52 and continues for 10 seconds. Concurrently, the second chock in the caving sequence at chock #53 persists for an additional 5 seconds, concluding at the 15-second mark. Figure 10(a) illustrates the dust particle flow pattern at 15 seconds, capturing the operation of two consecutive caving chocks at chocks #53 and #55. In addition to the dust induced from the upstream caved chock #51, further dust is generated from the caving chocks #53 and #55, covering the rear AFC regions of chocks #51-57 and the walkway of chocks #52-60.

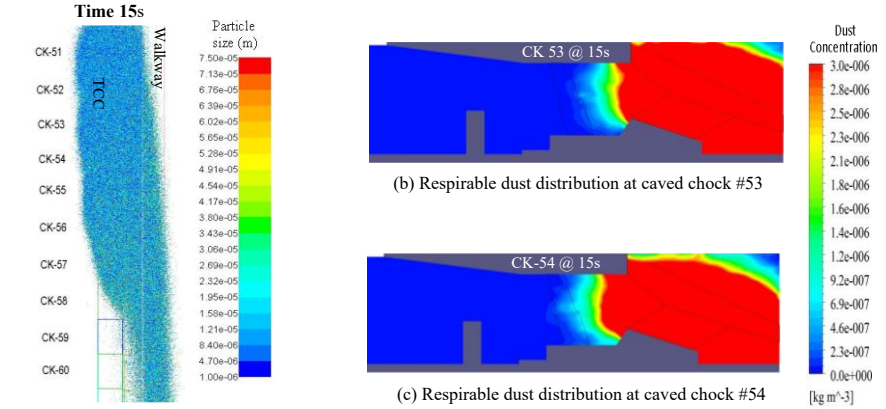

(a)Inhalable dust particle flow pattern at 15s

(b) Respirable dust distribution at caved chock #53

(c) Respirable dust distribution at caved chock #54

Figure 11 Caving dust flow pattern and dust distribution at 15s

Respirable dust above rear AFC reach the face height and small size particles starts to move in normal to the flow direction at chock #53, #54 and #55 which can be observed from the dust distribution indicated in Figure 11 (b), and Figure 12 the respirable dust reach above 2.5mg/m³ in the walkway.

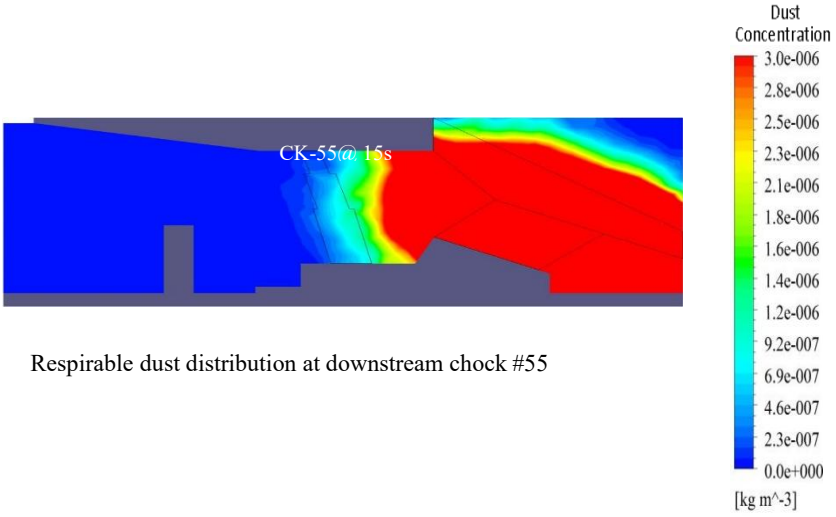

Respirable dust distribution at downstream chock #55

Figure 12 Caving dust distribution at downstream chocks at 15s

In Figure 13, the patterns of dust flow and distribution are depicted at the 20-second mark, coinciding with the initiation of the fourth caving in the sequence at chock 52 for a duration of 5 seconds, and the completion of the third caving in the sequence at chock

55. Figure 13 (a) clearly shows that dust particles blanket the walkway of downstream chocks 53-61, while particles are left in the rear AFC regions of these chocks. Notably, at caving chock 52, there is no caving operation on the upstream side, and the walkway of chock 52 is partially covered with dust, displaying very low respirable dust, as depicted in Figure 13 (b).

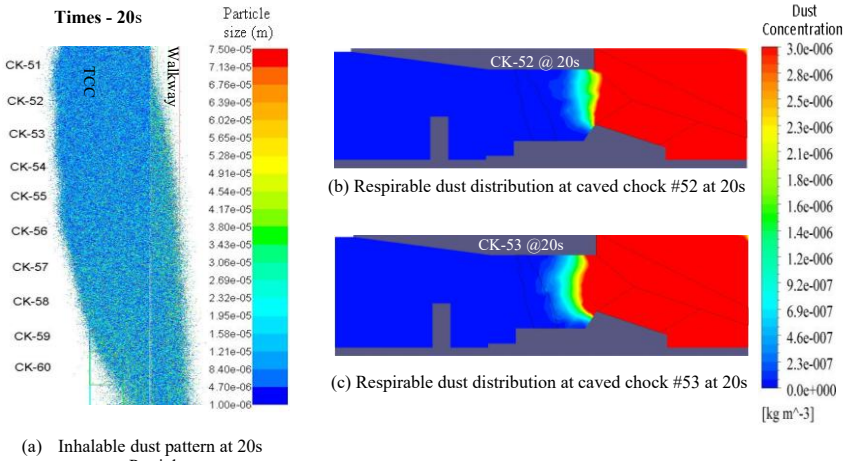

(a) Inhalable dust pattern at 20s

(b) Respirable dust distribution at caved chock #52 at 20s

(c) Respirable dust distribution at caved chock #53 at 20s

Figure 13 Caving dust flow pattern and distributions at caved chock #52 at 20s

In Figure 14(a), the walkway of the caving chock 55 is completely filled with high concentrations of 3mg/m^3 and the concentrations in the walkway of the 3rd caving chock in sequence chock 55 is due to migration of particles from the upstream side of the 2nd and 4th caving supports 52 and 53.

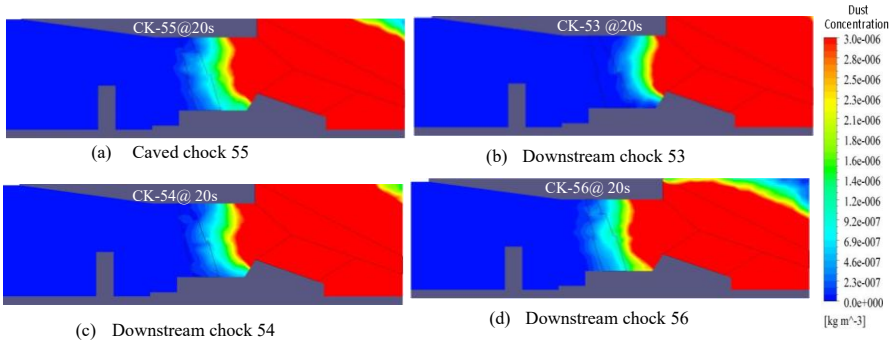

(a) Caved chock 55

(b) Downstream chock 53

(c) Downstream chock 54

(d) Downstream chock 56

Figure 14 Caving dust flow patterns at caved and downstream chocks

21-30s

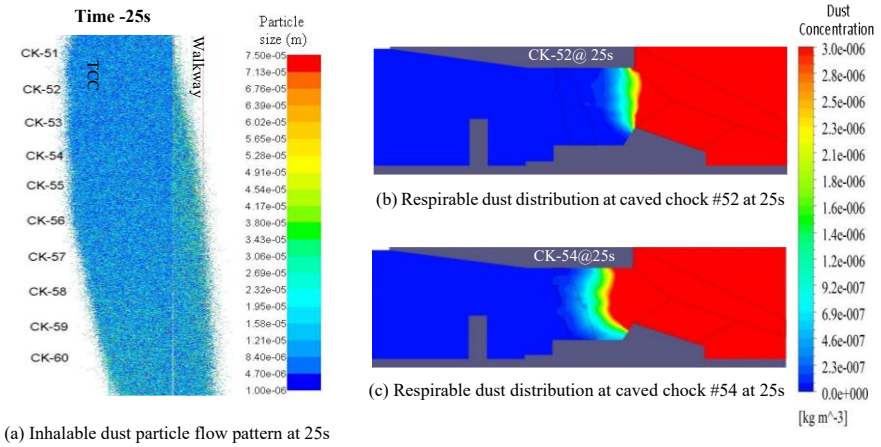

(a) Inhalable dust particle flow pattern at 25s

(b) Respirable dust distribution at caved chock #52 at 25s

(c) Respirable dust distribution at caved chock #54 at 25s

Figure 15 Caving dust flow pattern and dust distributions at caved chock#52 and #54 at 25s

During 21-30s, 4th caving in sequence at chock #52 continues to cave till 25ths. From 20th s, 5th caving in sequence initiates at the chock #54 and caves for 10s. This completes one full caving cycle involving five chocks #51, #52, #53, #54 and #55. Figure 15(a) indicates dust particles cover the walkway and the rear AFC of the downstream chocks 53-60 and Figure 15(b) indicates respirable dust concentration in the walkway of the caved chock #52 with concentrations below 1mg/m³ and only a fraction of the walkway exposed to respirable dust. Figure 15(c) indicates high respirable dust of 2.5mg/m³ in the walkway of the caving chock #54.

At 25s, high respirable dust above 3mg/m³ is observed in most of the walkway regions of the downstream chocks #55, #56 and #58 as indicated in Figure 16. At 30s, high dust concentration above 3mg/m³ is observed in the walkway region of the downstream chocks 55-60 as indicated in Figure 17 and Figure 18.

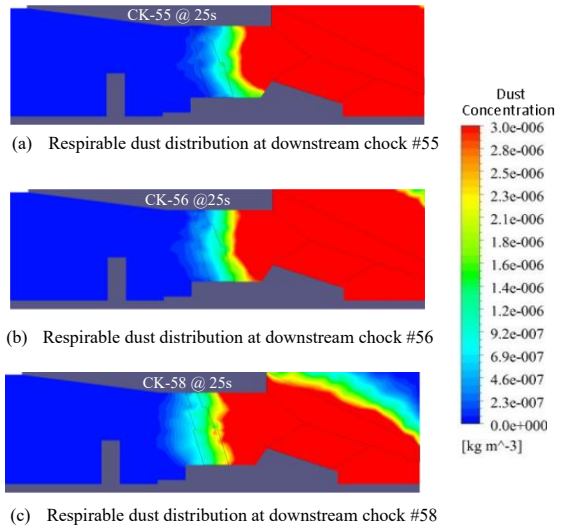

(a) Respirable dust distribution at downstream chock #55

(b) Respirable dust distribution at downstream chock #56

(c) Respirable dust distribution at downstream chock #58

Figure 16 Caving dust distribution at downstream chocks at 25s

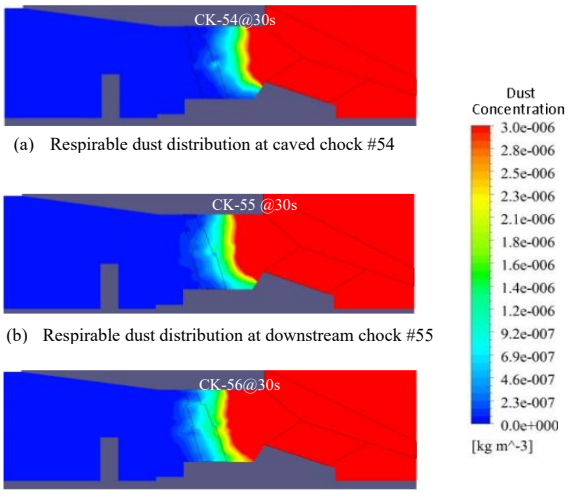

(a) Respirable dust distribution at caved chock #54

(b) Respirable dust distribution at downstream chock #55

(c) Respirable dust distribution at downstream chock 56

Figure 17 Caving dust distribution at caved chock 54 at 30s

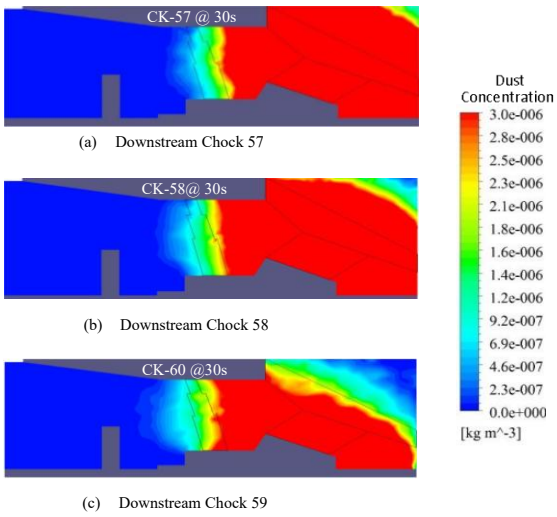

Figure 18 Caving dust distribution at downstream chock 60 at 30s

7 CONCLUSION

In summary, the investigation into transient caving dust modeling aimed to understand the flow patterns of dust during the sequential caving operation across the LTCC face over a 30-second duration. The analysis, conducted at 5-second intervals during the caving operation, focused on the caved chock and its downstream counterparts. Results revealed that respirable dust would partially cover the walkway of the first two chocks (51 and 52), with concentrations remaining below 2mg/m³. Notably, elevated respirable dust of 2.5mg/m³ are consistently observed in the walkway regions of the 3rd, 4th, and 5th caved chocks (53, 54, and 55) throughout the entire 30-second caving cycle.

Furthermore, the study highlighted the migration of respirable dust particles from the rear AFC into the walkway of downstream chocks. Chocks 56 to 60 are found to contain high respirable dust above 3mg/m³. The analysis also pointed out that the ventilation air carried respirable dust over long distances to the downstream chocks, emphasizing the need for comprehensive dust control strategies beyond the caving chock. It is noted that during a single caving cycle, the rear AFC experienced high respirable dust exceeding 3mg/m³, with limited dispersion due to low air velocities in these areas.

The findings underscore the importance of implementing effective dust control measures not only at the caving chock but also at the downstream chocks to prevent air contamination in the walkway. Overall, this study provides valuable insights into the dynamics of respirable dust dispersion during LTCC face caving operations, offering a

foundation for developing targeted strategies to mitigate potential health and safety risks associated with dust exposure.

Airflow patterns in the LTTC face vary significantly at the MG entrance, mid face, and in the TG exit region. This has a significant impact on the caving dust flow patterns. Future work could extend this model to account for variable airflow patterns by incorporating the effects of the caving sequence near the main gate (MG) region and the tailgate (TG) corner areas.

REFERENCES

QUANG, D.H., 2010. The effect of seam dip on the application of the longwall top coal caving method for inclined thick seams. PhD thesis. University of New South Wales.

CAI, Y., BRUCE, B., HEBBLEWHITE, U., ORNDER, B., XU, M., KELLY, M. and WRIGHT, B., 2004. Application of Longwall Top Coal Caving to Australian Operations. ACARP Project C11040.

TANGUTURI, K., BALUSU, R. and MORLA, R., 2014. CFD modelling of methane gas distribution and its control strategies at the tailgate region. Journal of Computational Multiphase Flows, 6(1), pp.65–77.

GREG, D., GLENN, S. and TIM, C., 2007. Top coal caving longwall maximizes thick seam recovery. World of Mining Professionals. Available at: http://www.womp-int.com/story/2007vol5/story025.htm [Accessed 11 Jul. 2025].

REN, T., QIAO, M., ROBERTS, J. AND HINES, J., 2023. Monitoring and computational modelling of ventilation and dust flow in development panel. In: 2023 Resource Operator Conference. University of Wollongong, Wollongong.

CRC Press, 2023. Development of VR-CFD-based training tool for dust control in gateroad development. In: Proceedings of the 19th North American Mine Ventilation Symposium, pp.330–337.

REN, T. and BALUSU, R., 2008. Innovative CFD modelling to improve dust control in longwalls. In: Proceedings of the Underground Coal Operators Conference, pp.137–142.

WORLD HEALTH ORGANIZATION (WHO), 1999. Hazard prevention and control in the work environment: Airborne dust. WHO/SDE/OEH/99.14. Geneva: WHO. Available at: http://www.who.int/occupational_health/publications/en/oehairborne dust.pdf [Accessed 11 Jul. 2025].

ANSYS, 2023. ANSYS 23.0 User Reference Manual.